



LAWRENCE
LIVERMORE
NATIONAL
LABORATORY

The Greenhouse Effect and Climate Feedbacks

C. Covey, R. M. Haberle, C. P. McKay, D. V. Titov

November 28, 2012

Comparative Climatology of Terrestrial Planets

Disclaimer

This document was prepared as an account of work sponsored by an agency of the United States government. Neither the United States government nor Lawrence Livermore National Security, LLC, nor any of their employees makes any warranty, expressed or implied, or assumes any legal liability or responsibility for the accuracy, completeness, or usefulness of any information, apparatus, product, or process disclosed, or represents that its use would not infringe privately owned rights. Reference herein to any specific commercial product, process, or service by trade name, trademark, manufacturer, or otherwise does not necessarily constitute or imply its endorsement, recommendation, or favoring by the United States government or Lawrence Livermore National Security, LLC. The views and opinions of authors expressed herein do not necessarily state or reflect those of the United States government or Lawrence Livermore National Security, LLC, and shall not be used for advertising or product endorsement purposes.

The Greenhouse Effect and Climate Feedbacks

Curt Covey

Lawrence Livermore National Laboratory

Robert M. Haberle

NASA Ames Research Center

Christopher P. McKay

NASA Ames Research Center

Dmitri V. Titov

European Space Agency

May 8, 2013

LLNL-BOOK-605012

This chapter reviews the theory of the greenhouse effect and climate feedback. It also compares the theory with observations, using examples taken from all four known terrestrial worlds with substantial atmospheres: Venus, Earth, Mars and Titan. The greenhouse effect traps infrared radiation in the atmosphere, thereby increasing surface temperature. It is one of many factors that affect a world's climate. (Others include solar luminosity and the atmospheric scattering and absorption of solar radiation.) A change in these factors—defined as climate forcing—may change the climate in a way that brings other processes—defined as feedbacks—into play. For example, when Earth's atmospheric carbon dioxide increases, warming the surface, the water vapor content of the atmosphere increases. This is a positive feedback on global warming because water vapor is itself a potent greenhouse gas. Many positive and negative feedback processes are significant in determining Earth's climate, and probably the climates of our terrestrial neighbors.

1. INTRODUCTION

The greenhouse effect occurs when short-wavelength solar radiation penetrates an atmosphere more readily than the long-wavelength infrared radiation (IR) emanating from the surface and from the atmosphere itself. *Fourier* (1827) pointed out that this effect would warm Earth's surface by trapping heat supplied by the Sun. He also noted that freely rising warm air—natural convection—would counteract the effect to some extent (so the greenhouse analogy is somewhat misleading). Subsequent nineteenth- and twentieth-century work beginning with laboratory measurements by *Tyndall* (1873) quantified IR absorption by water vapor, carbon dioxide (CO₂) and other atmospheric constituents. *Arrhenius* (1896) and *Calendar* (1938) then computed surface temperature increases due to atmospheric CO₂ produced by fossil fuel burning. These were only hypothetical increases because the ocean could potentially absorb nearly all of the CO₂. But when *Revelle and Suess* (1957) demonstrated that a substantial fraction of human-produced CO₂ remains in the atmosphere, longstanding theory then implied that global warming would follow.

Although human-induced global warming (a change of temperature) is logically distinct from the natural greenhouse effect and its influence on equilibrium steady-state temperature, the two processes are related. Indeed, as observations of human-produced atmosphere CO₂ accumulated (*Keeling*, 1976), spacecraft observations of Venus found both a massive CO₂ atmosphere and an extremely hot surface (*Hunten and Goody*, 1969; *Pollack et al.*, 1980). Modern observations have confirmed natural greenhouse effects on

Earth and other worlds (*Houghton, 2002*) as well as “very likely” anthropogenic global warming on Earth during recent decades (*Solomon et al., 2007*).

The greenhouse effect is only one of many factors that determine climate. Solar luminosity is the ultimate energy source of a world unless its internal heat sources are significant. Atmospheric gases, cloud particles, aerosols (other suspended particles) and the surface absorb and scatter solar radiation as well as IR; at the temperatures considered in this chapter they also emit significant amounts of IR. Therefore any change of solar behavior, atmospheric constituents or surface properties can potentially change weather and climate. Traditionally such changes are divided into “forcing factors” external to the system under consideration (e.g. solar luminosity variations, asteroid and comet impacts, volcanic eruptions) and “feedback processes” that result from the initial climate change due to the forcing factors. Feedback can either be positive or negative, i.e. either reinforcing or counteracting the initial climate change.

This chapter applies the above concepts to the four known terrestrial worlds possessing substantial atmospheres: Venus, Earth, Mars and Titan. In this chapter a “terrestrial” world is defined as mainly rocky in composition, thus excluding the large gaseous and watery planets, and “substantial atmosphere” means (rather arbitrarily) a surface pressure ≥ 1 mbar, thus excluding Triton. It so happens that none of the four selected worlds possesses internal heat sources large enough to directly affect its global weather and climate.

2. RADIATIVE BALANCE AND GLOBAL TEMPERATURE

2.1. The greenhouse effect and global energy balance

2.1.1. Wavelength dependence of IR emission. Spacecraft observing Earth and other terrestrial worlds detect atmospheric IR absorption at the wavelengths and intensities predicted by molecular physics. Figures 1 – 3 follow *Pierrehumbert* (2011) in illustrating this principle for Earth, Venus and Mars respectively. Figure 1 shows an early weather satellite’s observation of IR looking down at the Mediterranean Sea in the absence of clouds (*Hanel et al.*, 1971). Sufficiently thick clouds (e.g. Earth’s liquid water clouds) absorb and emit IR as blackbodies, interacting with IR to the maximum possible extent. In contrast, the main gaseous components of an atmosphere often do not interact with IR significantly. Interaction is normally weak for diatomic molecules like oxygen (O₂) and nitrogen (N₂) that have relatively few rotational and vibrational degrees of freedom. More complex molecules like CO₂, methane (CH₄), ozone (O₃), nitrous oxide (N₂O) and water vapor (H₂O) can dominate the greenhouse effect under clear-sky conditions, even if they are present only in trace concentrations. This process is evident in the figure.

In addition to observed outgoing IR intensity (energy flux per unit area per unit solid angle) Figure 1 plots the Planck blackbody function $2hc^2\bar{\nu}^3 / \exp(hc\bar{\nu} / kT) - 1$ as a function of inverse wavelength ($\bar{\nu}$) for several values of temperature (T). IR intensities observed in “window” regions of the spectrum, at wavelengths for which trace gas absorption is negligible, are consistent with blackbody emission directly from a surface

with $T > 280$ K. In contrast, intensities where absorption from various trace gases is significant—as marked in the figure—are lower and correspond to colder temperatures. The most prominent minimum in effective radiating temperature is $T = 220$ K in the CO_2 absorption band centered at $\bar{\nu} = 670 \text{ cm}^{-1}$ (around $15 \text{ }\mu\text{m}$ wavelength). “That dip represents energy that would have escaped to space were it not for the [IR] opacity of CO_2 ” (Pierrehumbert, 2011). $T = 220$ K is a temperature characteristic of the lower and middle stratosphere. Figure 1 thus shows that at wavelengths near $15 \text{ }\mu\text{m}$, IR emission originates mainly from the stratosphere, because emission from lower levels of the atmosphere is prevented from escaping to space. This is direct evidence of the CO_2 greenhouse effect.

Figure 2 shows analogous spacecraft data from Venus. (Note the scale expansion for near-IR frequencies $\nu > 1500 \text{ cm}^{-1}$, corresponding to wavelengths $< 7 \text{ }\mu\text{m}$. This part of the spectrum is an informative diagnostic of lower atmospheric and surface conditions, although its energy fluxes are small compared with the longer wavelength thermal-IR region.) *In situ* observations by a long series of American and Soviet space probes have found that T exceeds 700 K near the surface under an atmosphere nearly 100 times more massive than Earth’s (Schubert, 1983). The observed effective radiating temperatures, however, lie in the range $220 - 260$ K, characteristic of the top levels of Venus’ planet-wide sulfuric acid (H_2SO_4) clouds. Nearly all IR from the hot surface and lower atmosphere is absorbed before it reaches the cloud tops. The clouds themselves are responsible for a good deal of this absorption, but the sharp minimum of IR intensity around 670 cm^{-1} in Figure 2 reveals that CO_2 plays a significant role as well—as expected since CO_2 is the major component in Venus’ atmosphere (96% by volume).

Indeed, radiative-convective computations (Section 2.1.3) suggest that CO₂ is the most important factor in the Venus greenhouse. Removing factors one at a time, *Titov et al.* (2007) find that by far the greatest greenhouse warming in their model is due to CO₂ (see their Table 5.1). Applying same procedure to Earth, *Schmidt et al.* (2010) identify H₂O as the most important greenhouse gas, with CO₂ and clouds tied for second place (see their Table 1). But Schmidt et al. also note that one-at-a-time removal of factors can be misleading in the presence of spectral overlaps. After taking this complication into account, they conclude “that water vapor is responsible of just over half, clouds around a quarter and CO₂ about a fifth of the present-day total greenhouse effect” on Earth.

Satellite data for Mars analogous to Figures 1 – 2 show the same sharp minimum due to CO₂ absorption. For example, a summer afternoon spectrum finds blackbody emission directly from the surface with $T \sim 270$ K in most wavelengths, but the effective emission T drops below 180 K at the center of the 670 cm⁻¹ CO₂ absorption band (Figure 3). This result is expected since the Martian atmosphere is 95% CO₂ by volume.

Analogous data for Titan—obtained by the same instrument that provided the Earth data in Figure 1—reveal only a trace of CO₂ but do find strong emission bands from CH₄ and other hydrocarbons, as well as pressure-induced absorption bands of molecular hydrogen (*Hanel et al.*, 1981, 1982; *Samuelson et al.*, 1983). The hydrocarbons and molecular hydrogen (H₂) make up small but important percentages of Titan’s atmosphere, which consists mainly of N₂. The pressure-induced absorption effect occurs because frequent collisions of H₂ with N₂ molecules lead to an enhancement of their IR absorption beyond the weak amounts normally expected of diatomic molecules (*Samuelson et al.*, 1981).

2.1.2. *Global mean energy balance.* Integrating the IR intensity escaping an atmosphere over all wavelengths and over all outward directions produces the energy flux of outgoing longwave radiation (OLR). Absent significant internal heat sources, global area- and time-averaged OLR must balance absorbed solar energy flux in a steady-state equilibrium climate. Spacecraft observations of terrestrial worlds confirm this balance. Even during the recent period of global warming on Earth, the imbalance is only a fraction of a percent (*Trenberth and Fasullo, 2010*).

The assumption of global mean energy balance leads to a simple assessment of the greenhouse effect. Given an incoming solar energy flux S and a direction- and wavelength-weighted planetary albedo α , absorbed solar energy flux is $(S/4)(1 - \alpha)$ per unit area. (The factor 4 is the ratio of total surface area, $4\pi r^2$, to the surface area of a disk intercepting S , πr^2 .) Setting $\text{OLR} = \sigma T_e^4$ then defines an effective global mean radiating temperature $T_e = \sqrt[4]{(S/4\sigma)(1-\alpha)}$. One would expect the global mean surface temperature T_{sfc} to equal T_e in the absence of an atmosphere (given the same value of α). Table 1 compares T_e with observed T_{sfc} for Venus, Earth, Mars and Titan. In all cases except Mars T_{sfc} exceeds T_e , indicating greenhouse warming. Judging the magnitude of the greenhouse effect by $T_{sfc} - T_e$, Venus exhibits by far the largest, but Earth's natural greenhouse effect is also important. Without it, our world's surface would be a frigid 255 K and probably devoid of life. Titan's surface pressure (proportional to mass per unit area) is greater than Earth's and its greenhouse effect is evidently appreciable, as expected for an atmosphere including CH_4 and other greenhouse gases. Surface pressure on Mars is just 1% the value on Earth, so only a small greenhouse warming might be expected even though the Martian atmosphere is nearly all CO_2 .

Of course there is more than one way to define the magnitude of the greenhouse effect. Rather than $T_{sfc} - T_e$ one might consider the amount of energy flux reaching the surface that is due to IR from the atmosphere. This amount is about 1/3 the total energy flux reaching the surface for Mars, a significant effect. For Earth, Titan and Venus the fractions are about 2/3, 9/10 and 999/1000 respectively (*Courtin et al.*, 1992). By this measure Titan's greenhouse is second only to that of Venus.

The Mars numbers in Table 1 actually show T_{sfc} slightly *less* than T_e , but this is an artifact of averaging nonlinear functions. The average of the 2nd power of a quantity ($\overline{x^2}$) always exceeds the average value raised to the 2nd power (\bar{x}^2). The average of the 4th power ($\overline{x^4}$) exceeds the average value raised to the 4th power (\bar{x}^4) as long as the asymmetry of variations is modest, which is the case for planetary surface temperature. Thus in general $\overline{\sigma T^4} > \sigma \bar{T}^4$, and the space-time averaging that produced the global mean numbers in Table 1 underestimates IR emission from the surface. Defining an effective surface temperature $\sqrt[4]{\overline{T^4}}$ overcomes the problem. This correction is evidently not needed for the more massive atmospheres of Venus, Earth and Titan, which moderate surface temperature changes, but for Mars it reverses the sign of $T_{sfc} - T_e$ (*Haberle*, 2013). The seasonal, day-to-night and equator-to-pole temperature contrasts on Mars are so large that direct observation of global means is difficult, and the Martian numbers in Table 1 come from a general circulation model (Section 3) whose output is consistent with available observations (*Haberle et al.*, 2010).

The varying number of digits in the other entries of Table 1 reflects varying accuracy of the observations. Values of S are obtained by scaling precise measurements

of Earth satellites (*Loeb et al.*, 2009) by the known distances to other worlds. Values of α are less accurate due to uncertainties in the angular distribution of outward reflected solar energy flux and its space-time dependence. For Venus, spacecraft measurements give a range of α from 0.75 to 0.82, with the lower values obtained more recently (*Titov et al.*, 2013). For Earth, extensive measurements suggest a 95% confidence interval of $\alpha = 0.28 - 0.32$ (*Covey and Klein*, 2010; but see *Kim and Ramanathan*, 2012 for a more precise claim). Other energy flux error bars are more difficult to quantify. With the exception of Mars, the temperature values in Table 1 come from *in situ* measurements: once for Titan (*Fulchignoni et al.*, 2005) several times for Venus (*Schubert*, 1983) and hundreds of thousands of times for Earth (*Jones et al.*, 1999). The observations are sufficiently accurate to unequivocally establish natural greenhouse warming on Venus, Earth and Titan, and to suggest a small greenhouse warming in the thin Martian atmosphere.

2.1.3. Radiative-convective equilibrium. The simpler climate models work with space-time averaged data. One can start with the latitude-, longitude- and time-averaged solar energy flux incident on the atmosphere (the single number $S/4$; see Section 2.1.2). This input and the approximations described below allow computation of temperature T as a function of altitude z only: a one-dimensional climate model (*Ramanathan and Coakley*, 1978). Given well-known interactions of greenhouse gas molecules with IR (Section 2.1.1) together with some reasonable assumptions about surface and cloud-particle interactions with IR and with solar radiation, upward and downward radiative energy fluxes are computed as a function of z . Natural convection is included as an additional upward energy flux; often this is done by simply adjusting the lapse rate $|\partial T / \partial z|$ to avoid exceeding an instability criterion. The critical lapse rate is generally reached

in the lower part of a sufficiently thick atmosphere because the blackbody emission function σT^4 increases linearly downward with optical depth (see e.g. Equation 2.15 in *Houghton, 2002*) and most optical depth is concentrated near the surface. The z -derivative of the total net energy flux gives a heating or cooling rate and thus the local rate of temperature change $\partial T / \partial t$. Temperature is then updated, the fluxes are recomputed and the process continued until convergence to a radiative-convective equilibrium $T(z)$ profile is obtained.

One might question the usefulness of a model that ignores the three-dimensional structure and circulation of an atmosphere, and accounts for turbulent vertical heat transport by the simplest possible convective adjustment. But one-dimensional models often produce results in agreement with space-time averaged observations (perhaps because vertical gradients are typically much larger than horizontal gradients in atmospheres). For example, *Manabe and Weatherald (1967)* created a one-dimensional model of Earth's atmosphere assuming current CO_2 , H_2O , O_3 and cloudiness. They obtained an equilibrium temperature $T(z)$ decreasing linearly from 288 K at the surface to about 210 K at $z \sim 15$ km, then increasing slowly through $z > 40$ km. The model's surface temperature agrees with averaged surface observations (*Jones et al., 1999*; see Table 1). Surface temperature would be much higher if convection did not carry heat upward (*Lindzen and Emanuel, 2002*) so the convective adjustment procedure evidently represents this heat transport appropriately. The altitude and the value of the model's $T(z)$ minimum agree with modern observations to within a few km and a few K respectively (see Figure 3.1a in *Eyring et al., 2010*).

Analogous models for Mars (*Marinova et al.*, 2005) and Venus reproduce the much smaller and much larger greenhouse effects, respectively, on these two worlds compared with Earth. The case of Titan includes an “anti-greenhouse” effect and will be discussed in the following section. Venus provides a severe challenge to climate models due to its atmosphere’s extreme temperatures, its mass (nearly two orders of magnitude greater than Earth’s atmosphere) and its ubiquitous cloud cover that absorbs nearly all of the incident solar radiation. The challenge is simplified, however, by the massive atmosphere’s tendency to equalize temperatures in space and time. One-dimensional models have obtained excellent agreement with $T(z)$ observed by numerous space probes between the surface and about 70 km altitude (the level of the cloud tops) although unresolved issues persist involving undetected or poorly measured aerosols and trace gases (*Pollack et al.*, 1980; *Crisp and Titov*, 1997; *Bullock and Grinspoon*, 2001). The consistent message of the models is that Venus’ high surface temperature (Table 1) arises primarily from the large amount of CO₂ in its atmosphere. Indeed, Table 1 shows that the effective radiating temperature T_e of Venus is less than that of Earth. By definition, this means that Venus absorbs *less* solar energy than Earth despite its orbit closer to the Sun, due to the high planetary albedo α arising from its clouds. The greenhouse potential of atmospheric CO₂ is thus incontestable.

2.2. Greenhouse vs. anti-greenhouse effects

What if the upper atmosphere absorbed all of the solar radiation that it did not reflect back to space, but at the same time had very little opacity in the IR? In that case

the upper atmosphere would radiate only a small amount of outgoing longwave radiation upward to space and an equal amount downward. Energy balance at the surface would then imply that $\sigma T_{sfc}^4 = OLR$, and essentially all of the surface IR emission would pass through the upper atmosphere and escape to space. Energy balance the top of the atmosphere would then imply that $(S/4)(1 - \alpha) \equiv \sigma T_e^4 = OLR + \sigma T_{sfc}^4$. Elimination of OLR between the two energy balance equations gives $\sigma T_e^4 = 2 \sigma T_{sfc}^4$: surface temperature is reduced from the effective radiating temperature by a factor $1 / 2^{1/4} = 0.84$. This reasoning is idealized not only by the assumed complete dominance of solar over IR opacity but also by the implicit separation of the atmosphere into two distinct layers. Nevertheless, the conclusion that surface temperature is reduced 16% below T_e indicates the possibility of a significant cooling effect. *McKay et al.* (1991) called this scenario an “anti-greenhouse effect” because it reverses the greenhouse scenario, in which atmospheric optical depth is greater in the IR than in solar energy wavelengths.

Figure 4 compares the anti-greenhouse with the greenhouse in schematic examples. In these examples we assume $\alpha = 0$ for simplicity. In the no-atmosphere case, all 3 units of incoming solar radiation are absorbed by the surface and re-radiated as OLR, and $T_{sfc} = T_e$. If an idealized purely greenhouse atmosphere is introduced, blocking IR with no effect on α , then an equilibrium eventually obtains in which 3 units of OLR are still emitted to space and T_e is unchanged. But now it is the atmosphere that emits the OLR, together with an equal amount of IR downward to the surface. Thus the surface receives a total of 6 units of energy flux from the combination of solar and IR—twice the amount received in the no-atmosphere case—and in equilibrium $T_{sfc} = 2^{1/4} T_e = 1.19 T_e$. As shown above, an idealized purely anti-greenhouse scenario gives $T_e = 0.84 T_e$. The

schematic example in the bottom picture in Figure 4 depicts an anti-greenhouse combined with a greenhouse effect. Again we assume that $\alpha = 0$, so at equilibrium the OLR and T_e are unchanged. But now we assume an upper atmosphere absorbs 2 of the 3 units of incoming solar radiation while a lower atmosphere blocks IR, re-radiating 2 units upward to space and an equal amount downward to the surface. As a result, the surface absorbs a total of 3 units of energy flux and $T_{sfc} = T_e$: in this example the greenhouse and anti-greenhouse effects cancel exactly.

McKay et al. (1991) found that on Titan, the greenhouse effect dominates, but the anti-greenhouse effect is significant. They obtained realistic numbers for Titan from Voyager spacecraft data together with a one-dimensional climate model; the numbers are consistent with subsequent Cassini-Huygens spacecraft data (*Fulchignoni et al.*, 2005; *Griffith*, 2009). On Titan the greenhouse effect is primarily due to pressure-induced IR absorption by N_2 , CH_4 and H_2 , while the anti-greenhouse effect is due to solar absorption by a high altitude hydrocarbon haze layer. Titan's effective radiating temperature is $T_e = 82$ K. The idealized extreme anti-greenhouse would reduce this by $(1 - 0.84) \times 82$ K = 13 K at the surface, but the actual anti-greenhouse on Titan reduces it by only 9 K. At the same time the greenhouse effect raises surface temperature by 21 K. The net result is that $T_{sfc} = 82 - 9 + 21 = 94$ K.

2.3. Radiative forcing, feedback, and climate response

Changing the factors that affect global energy balance (Table 1) will in general change surface temperature and other aspects of a planet's climate. In studying this

process, it is useful to define radiative forcing (ΔF) as the change in net energy flux at the top of the atmosphere that *would* occur *if* a given factor changed more or less instantaneously with all other climate conditions (temperature, winds, etc.) remaining constant. For example, $\sim 0.1\%$ peak-to-peak variations of solar luminosity have been observed over the last few sunspot cycles, implying $\Delta F \sim (0.001)(S/4)(1 - \alpha) \sim 0.2 \text{ W m}^{-2}$ averaged over Earth's surface. This number may be compared with $\Delta F \equiv \Delta F_{2\times\text{CO}_2} \sim 4 \text{ W m}^{-2}$ for a hypothetical sudden doubling of atmospheric CO_2 (Forster *et al.*, 2007).

Some cautionary and clarifying points are in order. First, for most factors ΔF is a hypothetical number not subject to direct observation (although it is computable from laboratory experiments and the standard theory of electromagnetic radiation). Second, as a single number, ΔF necessarily omits variations in space-time and other details. For example, the above-noted 0.1% variations of S include much larger relative variations in the ultraviolet range of the spectrum; these can affect O_3 and temperature in the stratosphere, which in turn may affect the climate near the surface (Gerber *et al.*, 2012). Finally, the phrase “more or less instantaneous” in the definition of ΔF is deliberately chosen. It allows ΔF to incorporate rapid processes that could be reasonably considered a part of climate forcing, such as interactions of aerosols and cloud particles (Forster *et al.*, 2007) or stratospheric temperature adjustment (Hansen *et al.*, 1981). Global climate change may then be separated conceptually into short-term forcing ΔF and long-term response, with the latter produced by a combination of ΔF and a variety of feedback processes. In the following subsections we consider examples of both forcing and feedback.

2.3.1. *Human perturbation of Earth's energy balance.* Observations demonstrate that CO₂ and other greenhouse gases in Earth's atmosphere are increasing at unprecedented rates. Figure 5 shows time series of CO₂, CH₄ and N₂O over the last 10,000 years. Each time series combines *in situ* atmospheric measurements for the recent past with measurements of air bubbles trapped in continental ice sheets for the more distant past. Unlike the components of urban smog, CO₂, CH₄ and N₂O are chemically stable enough to be well mixed globally, so the difference between local measurements and the global average is not an issue. The sharp concentration upturns of all three gases around the time of the Industrial Revolution is *prima facie* evidence of a human origin. The data are consistent with fossil fuel burning and other human activities such as forest clearing and agriculture. For CO₂, the record of fossil fuel use provides more than enough carbon emission to account for the atmospheric increase. The total amount of carbon produced by fossil fuel burning over the last two centuries corresponds to roughly twice the atmospheric CO₂ increase during that time. This implies that about half the emitted CO₂ has been absorbed by the ocean and the biosphere (or more than half, if forest clearing and agriculture contributed an appreciable fraction of CO₂ emissions).

The increasing greenhouse gases shown in Figure 5 imply a radiative forcing ΔF associated with each gas. By this measure, CO₂ is the most important greenhouse gas emitted by human activity. Taking the beginning of the Industrial Revolution (c. 1750) as a starting point, ΔF from CO₂ exceeds ΔF from CH₄ by more than a factor of 3, which in turn exceeds ΔF from N₂O by about a factor of 3 (see Table 2). Although CO₂ absorption is saturated near the center of the 15 μm band, adding CO₂ to the atmosphere increases heat trapping by broadening the absorption band to include a wider range of wavelengths

(see Figure 1). This effect leads to an approximate logarithmic dependence of ΔF on atmospheric CO₂ increase, in contrast to a stronger (square-root or linear) dependence for CH₄, N₂O, O₃ and chlorofluorocarbons (CCl₂F₂, etc.) whose IR absorption is less saturated at band centers (*Dickinson and Cicerone, 1986*).

Table 2 shows that human greenhouse gas emissions have put Earth well on the way to an effective doubling of atmospheric CO₂ ($\Delta F_{2\times\text{CO}_2} \sim 4 \text{ W m}^{-2}$). The combined ΔF due to CO₂, CH₄ and N₂O is $2.30 \pm 0.23 \text{ W m}^{-2}$ (90% confidence interval; *IPCC, 2007*). Also—as shown in Figure 1—O₃ is a greenhouse gas, and human activities affect it. Air pollution has increased O₃ in the lower atmosphere (the troposphere) while human-produced chlorofluorocarbons have decreased O₃ in the stratosphere. ΔF from O₃ is less precisely quantified than ΔF due to CO₂, CH₄ and N₂O because O₃ is not well mixed in the atmosphere, but its human-induced changes together with the chlorofluorocarbons (themselves potent greenhouse gases) may contribute up to an additional 1 W m^{-2} . Finally, carbon-rich sooty pollutants probably exert a small warming effect when deposited onto snow and ice surfaces ($\Delta F \sim 0.1 \text{ W m}^{-2}$).

Some other human activities exert a cooling effect on climate. Over the past few centuries an appreciable fraction of Earth's land surface area has been converted from forests to croplands and pastures (see Figure 2.15 in *Forster et al., 2007*). Consequent surface albedo increases may subtract up to 0.4 W m^{-2} from ΔF . Aerosol droplets containing H₂SO₄, originating from sulfur-containing pollutants, also exert cooling effects: both by direct backscattering of solar radiation to space, and by indirect effects that brighten and otherwise alter clouds. Aerosol / cloud interactions remain extremely uncertain because they involve both natural processes and measuring techniques that span

many orders of magnitude in spatial scale (*Penner et al.*, 2011; *McComiskey and Feingold*, 2012; *Stevens and Boucher*, 2012). The combined direct and indirect effects of aerosols could subtract between ~ 0.5 and 2 W m^{-2} from ΔF .

The grand total of human-induced ΔF is positive with a 90% confidence interval of $0.5 - 2.5 \text{ W m}^{-2}$ and a most likely value of 1.6 W m^{-2} (*Forster et al.*, 2007). The most likely value is just 0.7% of absorbed solar energy flux $(S / 4)(1 - \alpha)$ but this value is substantially larger than ΔF due to variations in solar luminosity. These variations are periodic, following the 11-year sunspot cycle, with positive and negative phases largely canceling. (The lack of a readily apparent 11-year periodicity in observed surface temperatures rules out the possibility of substantial effects on global climate that are indirectly catalyzed by phenomena connected with the solar cycle, such as magnetic and cosmic ray fluxes.) Long-term solar variability probably contributes a ΔF of only $\sim 0.1 \text{ W m}^{-2}$. Large volcanic eruptions, however, can temporarily create enough H_2SO_4 droplets in the stratosphere to reverse the human-induced upward trend in ΔF for a year or two and induce a small but measureable cooling effect for decades thereafter (*Gleckler et al.*, 2006).

In short, human perturbation of Earth's energy balance is almost certainly exerting a net warming effect ($\Delta F > 0$) and, over multi-decadal time scales, is larger than natural perturbations from solar variability and volcanic eruptions.

2.3.2. Water vapor feedback and related processes. A subtle assumption in the one-dimensional model of *Manabe and Weatherald* (1967) and many related Earth climate models was to fix not atmospheric H_2O concentration *per se*, but relative humidity: the ratio of H_2O concentration to its saturation value. Correspondingly the

threshold value of lapse rate that initiates convective adjustment was reduced in magnitude to a value appropriate for moist convection. In moist convection, condensation of water vapor or another volatile substance releases latent heat above the surface and thereby adds to upward heat transport (see e.g. Section 3.2 in *Houghton*, 2002). This reduction in lapse rate would by itself tend to reduce the surface warming due to an enhanced greenhouse effect. But constant relative humidity implies that the average water vapor content of the atmosphere increases with increasing T . Since H_2O is a potent greenhouse gas, a positive feedback effect would then occur. The combined lapse rate and water vapor feedback in climate models is invariably positive. Manabe and Weatherald found that with constant relative humidity the global mean equilibrium warming due to doubled CO_2 in Earth's atmosphere ($\Delta T_{2\times CO_2}$) would be about 2 K. Under the assumption that to first approximation a climate response depends on the value of ΔF but not on its physical origin, $\Delta T_{2\times CO_2}$ has become a standard measure of global climate sensitivity to any external forcing. The value of $\Delta T_{2\times CO_2}$ obtained by Manabe and Weatherald lies within the likely range inferred by a variety of modern techniques, including more realistic three-dimensional general circulation modeling (see Section 3 below).

In the early history of Venus, water vapor feedback may have been strong enough to preclude any equilibrium climate short of boiling away oceans and losing the hydrogen in H_2O to space: a “runaway greenhouse.” This concept was first quantified by *Komabayashi* (1967) and *Ingersoll* (1969) using one-dimensional climate models and later elaborated by many investigators (e.g. *Shaviv et al.*, 2011; *Kurokawa and Nakamoto*, 2012; *Hansen et al.*, this volume). Although it is necessarily speculative, the

possibility of a runaway greenhouse follows naturally from inspection of a phase diagram for water (*Ingersoll*, 1969). The same phase diagram illustrates why open bodies of liquid water can be common on Earth but must be essentially nonexistent on (present-day) Mars. On Earth, atmospheric pressures and temperatures lie well within the domain of liquid water's existence. On Mars, temperatures rarely exceed the freezing point and atmospheric pressures lie near the lower limit for liquid water's existence. Since the pressure is not due to H₂O vapor itself (but rather comes from CO₂) any liquid water exposed to atmosphere must quickly evaporate (e.g. *Hartmann*, 2005, Chapter 13).

Water vapor feedback is one example of a general process in which significant IR opacity comes from a gas whose atmospheric concentration depends on cycles of evaporation and condensation. This means that the gas concentration is controlled by coexistence with solid or liquid phases through the strong exponential dependence of vapor pressure on temperature. Both water vapor and carbon dioxide are involved in this process on Mars (see the following subsection). A similar positive feedback arises in Titan's atmosphere from the trace gas CH₄, which plays a role analogous to H₂O in Earth's atmosphere (*McKay et al.*, 1992; *Griffith*, 2009). Both liquid and vapor phases of CH₄ exist on Titan with ~ 45% relative humidity in the equatorial atmosphere (*Fulchignoni et al.*, 2005) while water vapor is frozen out. *McKay et al.* (1993) found that CH₄ feedback on Titan is about twice as strong as water vapor feedback on Earth due to (1) a steeper dependence of vapor pressure on temperature and (2) stronger pressure-induced IR absorption..

2.3.3. Orbital effects and feedbacks. A planet's orbit about the Sun and the orientation of its spin axis (obliquity) can vary due to gravitational perturbations of other

planets. Orbital variations give rise to variations both of global- and annual-mean S (from eccentricity changes) and of the distribution of incoming solar radiation as a function of latitude and season (from obliquity and precession changes). These energy flux variations have long been suspected of triggering Earth's ice ages, although it is not obvious how such very small forcing amplifies to produce dramatic climate change (see FAQ 6.1 in *Jansen et al.*, 2007). Mars may provide a more clear-cut example of orbital effects on climate (*Toon et al.*, 1980).

Three research developments encourage the study of ice age analogs on Mars (*Haberle et al.*, 2013). First, spacecraft have increasingly scrutinized the planet's geologic record, revealing a variety of ice-related deposits that cannot be produced in today's Martian climate. Second, the increasing realism of atmospheric general circulation models (Section 3) applied to Mars permits a more sophisticated interpretation of the geologic record. Third, variations in Martian orbital properties are predictable and much larger than for other Solar System bodies (due to the lack of a large stabilizing moon, and the proximity of massive Jupiter). Calculations show that Martian obliquity has varied between 15° and 45° and the eccentricity between 0 and 0.12 during the past 20 million years (*Laskar et al.*, 2004; by definition obliquity = 0° when the planet's spin axis is perpendicular to its orbit plane). Beyond that point, the calculations become chaotic but obliquity excursions as high as 80° are possible. These variations lead to large changes in the latitudinal and seasonal distribution of solar radiation that can mobilize and redistribute volatile reservoirs.

The two main exchangeable volatiles are CO_2 and H_2O . CO_2 may be adsorbed at the surface (*Keiffer and Zent*, 1992) or buried as ice below the surface near the South

Pole (*Phillips et al.*, 2011). Taken together, these two sources can store the equivalent of between $\sim 5 - 30$ mbar of CO_2 (i.e., $\sim 1 - 4$ times the current atmospheric mass). Water ice is known to exist at the surface near the North Pole, and in the subsurface at middle and high latitudes (*Boynton et al.*, 2002). These two sources represent a combined equivalent of at least ~ 10 m thick layer of globally distributed H_2O ice. Mobilization of CO_2 and H_2O as Martian climate warms would be roughly analogous to the H_2O and CH_4 vapor feedback processes discussed above for Earth and Titan respectively.

Obliquity variations produce the largest variations in received solar radiation and have received most of the attention in studies of recent Martian climate change. At times of high obliquity ($> 35^\circ$) the polar regions warm, volatile reservoirs are destabilized and surface pressures and humidities rise. The magnitude of the climate change is model dependent, but a doubling of surface pressure and an order of magnitude increase in the H_2O content of the atmosphere are plausible outcomes. Under these circumstances the greenhouse effect is strengthened and mean annual surface temperatures increase. However, the increase including only these vapor feedbacks is limited to a few K since the thin atmosphere does not significantly pressure-broaden the IR absorption lines, and atmospheric H_2O content is limited by the relatively low temperatures.

Cloud feedback could further amplify warming at high obliquity. Martian clouds tend to form at high cold altitudes, and climate models predict that they would increase in the high obliquity atmosphere. This could lead to an increasing cloud greenhouse effect. Modeling studies suggest that the clouds can potentially warm surface temperatures by 10s of K (*Haberle, et al.*, 2012; *Madeleine et al.*, 2013). But as with Earth (Section 3.2) cloud feedbacks are a major source of uncertainty in Martian climate models. Another

complication is dust storms, which should increase in frequency at high obliquity. How the dust cycle couples to the water and CO₂ cycles at times of high obliquity is unclear.

The opposite situation prevails at low obliquity. The atmosphere condenses at the poles and permanent polar CO₂ ice caps form. The surface pressure is then dictated by the polar energy balance (*Leighton and Murray, 1966*) and can fall to less than 1 mbar at 15° obliquity (*Wood et al., 2012*). In this regime, atmospheric water vapor declines and dust storms cease so that the atmosphere should be relatively aerosol-free. The climate at low obliquity is therefore dictated mostly by the radiative balance of an airless body.

2.3.4. Time variations. The term “equilibrium” has occurred frequently in the discussion so far. It means that time variations are slow enough that departures from global mean energy balance (Section 2.1.2) may be neglected. If this assumption is not valid, then one must consider the heat capacity of the climate system and (at least conceptually) the energy balance equation $(S / 4)(1 - \alpha) = OLR$ must be replaced by a temperature evolution equation. Such cases arise particularly on Earth, where the thermal inertia of the ocean is huge. One example is provided by volcanic aerosols (q.v.), which are removed from the atmosphere faster than the climate system can adjust to them. Two more dramatic examples are discussed below:

Pollack et al. (1983) computed the temporary cooling caused by a debris cloud following impact of a large asteroid or comet with Earth, which would block solar energy from the surface. This scenario is a massively enhanced version of the volcanic cooling mentioned above. *Pollack et al.* interpreted their one-dimensional model output to “represent a region near the impact site” rather than a global horizontal average. They considered two very different types of lower boundary condition: land surface that adjusts

instantaneously to near-surface air temperature, and a well-mixed upper ocean layer of depth $\Delta z = 75$ m. In the ocean case the surface temperature response is buffered by the heat capacity of water $\rho c = 4 \times 10^6 \text{ J m}^{-3} \text{ K}^{-1}$, and the time scale for initial cooling is $(\rho c \Delta z) (288 \text{ K}) / (S/4)(1 - \alpha) \sim 10$ years. Numerical results of Pollack et al. featured 40 K cooling in the land case, peaking 2 – 5 months after the impact, but only a few K cooling in the ocean case, extending well beyond 2 years. These results are plausible for mid-continental and open ocean areas respectively. Quantitative consideration of important issues such as land-sea heat transport and the effect of seasons, however, require three-dimensional modeling (*Toon et al.*, 1997).

Similar one-dimensional computations led to the concept of “nuclear winter.” *Turco et al.* (1983) argued that worldwide smoke would arise (literally) from cities burning in the wake of a major nuclear war. The smoke could intercept over 90% of solar energy flux well above the surface, so that land areas would cool sharply within a few weeks. The amount of land surface cooling predicted by the *Pollack et al.* (1983) one-dimensional climate model varied from 5 K to 40 K depending on the war scenario and assumptions about smoke production and smoke optical properties. The same inherent limitations of one-dimensional modeling noted above for impact scenarios also apply to nuclear winter. Three-dimensional general circulation simulations have not changed the basic conclusion that mid-continental areas would suffer rapid cooling; indeed they imply that even a “minor” nuclear war could lead to drastic climate change (*Robock*, 2011). Fortunately these predictions remain untested by direct real-world observations.

Temporary cooling in the asteroid impact and nuclear winter scenarios is related to the permanent cooling of the anti-greenhouse effect (Section 2.2). *Pollack et al.* (1983)

noted that their land climate “cools because it receives virtually no sunlight . . . despite the greatly enhanced infrared opacity of the atmosphere.” The net result is that “surface temperature tends asymptotically toward the effective temperature at which the planet radiates to space” $T_e \sim 290 \text{ K} - 40 \text{ K} \sim 250 \text{ K}$ (see Table 1). This is not, however, as much cooling as in the “pure” anti-greenhouse scenario, for which infrared opacity is negligible and surface temperature falls below T_e .

2.4. Non-linear combination of feedback terms

Any realistic examination of a world’s climate must deal with several different feedback processes at once. In addition to water vapor and analogous volatiles (Section 2.3.2) climate models of Earth and other terrestrial worlds have incorporated a long list of both positive and negative feedback ingredients. Rather than attempting to enumerate them, the following discussion emphasizes how they are distinguished from forcing and how they interact with each other.

By definition, feedback processes arise from the climate change induced by a separate initial forcing ΔF , amplifying the initial change (positive feedback) or diminishing it (negative feedback). The distinction between forcing and feedback is somewhat arbitrary. For example, one may assume an increase of atmospheric CO_2 as input to a climate model, as in Section 2.3.1 and *Pollack et al.* (1987) for Earth and Mars respectively. In this case atmospheric CO_2 provides the forcing. But it is a feedback in the Mars climate models of Section 2.3.3, and an “Earth system model” that includes the biosphere and ocean chemistry may take human CO_2 emissions as input, producing

atmospheric CO₂ concentration together with climate as output. In this case the carbon cycle becomes a feedback process (likely positive; see *Denman et al.*, 2007). On very long time scales, natural CO₂ emission from volcanoes and the removal of atmospheric CO₂ by rock weathering can together create a negative feedback loop (*Walker et al.*, 1981; *Goudie and Viles*, 2012).

Albedo provides one example of how feedback may be quantified. Figure 6 schematically shows how global mean absorbed solar radiation $(S/4)(1 - \alpha)$ and OLR (Section 2.1.2) may vary as a function of global mean surface temperature. One would normally expect that OLR increases with increasing T_{sfc} and also curves upward, i.e. both $\partial(OLR) / \partial T_{sfc}$ and $\partial^2(OLR) / \partial T_{sfc}^2$ are positive (unless a runaway greenhouse happens). The figure shows this behavior for both present-day and twice present-day concentrations of atmospheric CO₂, with the latter curve lowered by $\Delta F = 4 \text{ W m}^{-2}$ (Section 2.3.1). Considering worlds like Earth and Mars on which bright surface ice melts or evaporates with increasing T_{sfc} , one might guess that absorbed solar energy flux $(S/4)(1 - \alpha)$ also increases with increasing T_{sfc} . The figure shows this behavior under the additional assumption that $(S/4)(1 - \alpha)$ approaches a maximum value when T_{sfc} becomes very warm and all ice disappears. With these assumptions, $\partial[(S/4)(1 - \alpha)] / \partial T_{sfc}$ is positive but $\partial^2[(S/4)(1 - \alpha)] / \partial T_{sfc}^2$ is negative. Cloud feedback (q.v.) also affects albedo and thus $(S/4)(1 - \alpha)$, although the resulting signs of $\partial[(S/4)(1 - \alpha)] / \partial T_{sfc}$ and $\partial^2[(S/4)(1 - \alpha)] / \partial T_{sfc}^2$ are not obvious.

Figure 6 thus illustrates how climate forcing due to doubled CO₂ in Earth's atmosphere leads to global mean warming $\Delta T_{2 \times \text{CO}_2}$ in the presence of positive surface-albedo feedback. Energy balance occurs whenever the OLR and $(S/4)(1 - \alpha)$ curves

intersect. Two intersections occur for each OLR curve, giving four equilibrium climate states. The pair of intersections at lower values of T_{sfc} , however, represents unstable climate equilibrium states. In these states, slight decreases of T_{sfc} lead to OLR exceeding $(S/4)(1 - \alpha)$ and slight increases of T_{sfc} lead to $(S/4)(1 - \alpha)$ exceeding OLR, so that small perturbations are amplified. Since they are not physically attainable, these states can be ignored. The opposite situation occurs for the pair of intersections at higher T_{sfc} , which represents stable climate equilibrium states. For these states the figure shows that lowering the OLR curve (enhancing the greenhouse effect) leads to increasing T_{sfc} . After the climate system is perturbed by ΔF , equilibrium is restored by compensating changes in OLR and $(S/4)(1 - \alpha)$. If changes in T_{sfc} are small compared with the thermodynamic absolute value of T_{sfc} then one may linearize the global energy balance condition $(S/4)(1 - \alpha) = \text{OLR}$ and obtain

$$\Delta F = \frac{\partial(\text{OLR})}{\partial T_{sfc}} \Delta T_{sfc} + \frac{S}{4} \frac{\partial \alpha}{\partial T_{sfc}} \Delta T_{sfc} \Rightarrow \Delta T_{sfc} = \frac{\Delta F}{\frac{\partial(\text{OLR})}{\partial T_{sfc}} + \frac{S}{4} \frac{\partial \alpha}{\partial T_{sfc}}}. \quad (1)$$

Equation (1) implies that equilibrium ΔT_{sfc} is proportional to ΔF . The proportionality constant enters as a sum of feedback terms in the denominator. In the absence of an atmosphere, only the Planck term $\partial(\text{OLR}) / \partial T_{sfc} = \partial(\sigma T_{sfc}^4) / \partial T_{sfc} = 4\sigma T_{sfc}^3 = 4\sigma T_e^3$ would appear in the denominator. Substituting $T_{sfc} = 255 \text{ K}$ for Earth (Table 1) gives a Planck term $3.8 \text{ W m}^{-2} \text{ K}^{-1}$. If this were the only feedback process operating, then taking $|\Delta F| \sim 4 \text{ W m}^{-2}$ would give $\Delta T_{2 \times \text{CO}_2} \sim 1 \text{ K}$. Including albedo feedback adds the term $(S/4) \partial \alpha / \partial T_{sfc}$ to the denominator. This term is negative in the case of surface albedo feedback discussed above, decreasing the magnitude of the denominator and

increasing ΔT_{sfc} . Separately, the water vapor feedback discussed above would reduce $\partial(OLR) / \partial T_{sfc}$ and further increase ΔT_{sfc} . Evidently a combination of processes in the *Manabe and Weatherald* (1967) model produced a net positive feedback that doubled ΔT_{sfc} ($= \Delta T_{2\times CO_2}$) from about 1 K to 2 K. Cloud feedbacks (not considered by Manabe and Weatherald) will in general affect both the $\partial(OLR) / \partial T_{sfc}$ and $(S / 4) \partial \alpha / \partial T_{sfc}$ terms in Equation (1).

An important feature of Equation (1) is that separate feedback processes combine *non-linearly*. For example, the effect of albedo feedback is more pronounced if water vapor feedback is strongly positive, i.e. if $\partial(OLR) / \partial T_{sfc}$ is relatively small. This makes identifying and quantifying different feedback processes a difficult endeavor (*Roe and Baker, 2007*). Nowadays the endeavor is pursued using detailed observations, often acquired by spacecraft, together with climate models that are considerably more complex and hopefully more sophisticated than those discussed above.

3. MODERN CLIMATE MODELS

3.1. The need for complexity

There are limits to the ability of one-dimensional climate models to simulate a real three-dimensional world. Some limits are obvious. A model with no geographical variation over Earth's surface cannot say much about different regional effects of global warming, for example. But other limitations are more subtle. Although a long-run global mean balance between absorbed solar and emitted OLR energy fluxes exists (Section

2.1.2) the two fluxes are often far out of balance locally. On both Earth and Venus, satellite observations clearly show that absorbed solar radiation exceeds OLR at low latitudes and that the reverse is true at high latitudes (*Schofield and Taylor, 1982*). These observations imply that the atmosphere (and in Earth's case the ocean) transports heat northward and southward away from the tropics and toward the poles. Much of Earth's poleward heat transport is accomplished by longitude-varying baroclinic waves that apparently have analogs on Mars (*Read and Lewis, 2004*) and perhaps on Titan as well (*Mitchell, 2012*). In Venus' atmosphere, a strong equatorial super-rotation is the most prominent observed feature of the circulation; it cannot be explained without invoking longitude-varying waves (*Gierasch et al., 1997*). On Earth, land-sea heat transport plays a significant role in the seasonal cycle (*Fasullo and Trenberth, 2008*) and other transient climate changes (section 2.3.4). Also, the distributions of clouds and other atmospheric constituents such as local pollutants vary strongly. Such considerations have led to application of three-dimensional atmospheric general circulation models (GCMs) to all four terrestrial worlds discussed in this chapter, including details of clouds, surface terrain, etc., despite the consequent strain on computer resources.

GCMs are closely related to numerical weather prediction models of Earth's atmosphere, but they are used for a different purpose (*Washington and Parkinson, 2005*). Predicting the weather on Earth involves carefully initializing a model with the best observations of current weather and then simulating the atmosphere's evolution over a period of at most a week or two. The object is a detailed forecast of the weather at each location on Earth. A GCM, in contrast, runs for much longer periods of (simulated) time, and the weather systems it predicts are considered valid only in a statistical sense. Initial

conditions are not as important as in weather prediction. The sort of question addressed by Earth GCM climate simulations is “Will my home state suffer drought more often later in this century?” rather than “Will it rain in my home town later this week?” GCMs are also used to explore fundamental questions concerning the maintenance of atmospheric thermal structure and circulation on Earth and other planets.

3.2. Conservation laws and subgrid-scale parameterizations

GCMs are computer programs that solve the partial differential equations expressing physical conservation laws for mass, momentum and energy. These include vertical heat transport: essentially a GCM creates a one-dimensional climate model (Section 2.2.1) at each of several thousand grid-points around the world and computes radiative and convective contributions to $\partial T / \partial t$. At the same time the GCM determines other contributions to $\partial T / \partial t$ arising from horizontal and vertical temperature advection. This leads to a self-consistent computation of winds and temperatures. A GCM simulation comes closer to “first principles” than simpler models. For example, instead of assuming any particular value of relative humidity, Earth GCMs compute the concentration of atmospheric water vapor using thermodynamic laws and the conservation of water mass.

It must not be thought, however, that GCM simulations are based only on precisely known laws of classical physics. The equations that express these laws are non-linear owing to the advection terms in which wind velocity \mathbf{v} multiplies other dynamical variables, e.g. temperature advection proportional to $\mathbf{v} \cdot \nabla T$. Solution of the equations

therefore entails numerical approximation in which discrete points on a three-dimensional lattice replace spatially continuous fields, and discrete time steps replace continuous evolution in time. Roughly 100 km horizontal spacing, a few km vertical spacing and time steps a few minutes long are used in today's GCMs. This numerical discretization in turn requires something to be assumed about phenomena at finer space-time scales.

Clouds in Earth's atmosphere provide the most studied and perhaps the most challenging example of sub-gridscale parameterization. They often vary over horizontal scales of order 1 km or less, so they cannot be explicitly simulated with horizontal grid points separated by $\sim 10 - 100$ km. Therefore Earth GCMs must use empirical parameterizations to derive the large-scale effects of clouds from large-scale explicitly simulated fields like ν , T and water vapor concentration. One important feedback effect of clouds involves planetary albedo. Since clouds are typically brighter than the underlying surface, they can produce either positive or negative climate feedback via the term $(S/4) \partial\alpha / \partial T_{sf}$ in Equation (1) depending on whether bright clouds decrease or increase, respectively, in a warmer climate. Cloud feedback can also operate by affecting OLR (both on Earth and—as discussed in Section 2.3.3—on Mars). The *Manabe and Weatherald* (1967) one-dimensional simulation of equilibrium climate sensitivity assumed fixed cloudiness and obtained $\Delta T_{2\times\text{CO}_2} = 2$ K (Section 2.2.2). Different assumptions embedded in different cloud parameterizations are the primary reason that $\Delta T_{2\times\text{CO}_2}$ varies roughly between 2 – 5 K among different climate models (see Box 10.2 in *Meehl et al.*, 2007).

3.3. Successes and limitations

Like their one-dimensional cousins, GCMs are subject to the following general warning about modeling complex systems (*Box and Draper*, 1987, p. 424): “Essentially, all models are wrong, but some are useful. However, the approximate nature of the model must always be borne in mind.” GCMs attempt to simulate details of climate and climate change on spatial scales of the order of a few grid-point spacings, or roughly a few hundred kilometers in horizontal dimensions. Sub-gridscale parameterizations, which all GCMs incorporate, aim to represent processes with space-time scales as small as micrometers and seconds. All of this is done over the full global extent of a world, and typically continued for at least several Earth-years of simulated time. Obviously models this complicated will make mistakes. Of course, the mistakes are not just simple ones that are readily corrected; they include the consequences (not all of them known) of inevitable approximations.

Judging whether a GCM is useful despite its mistakes depends, of course, on the problem to which the model is applied. As the name “general circulation model” indicates, one goal is fundamental understanding of the mechanisms creating and maintaining an atmosphere’s general large-scale circulation. A useful start toward this goal was achieved by the first very Earth GCM (*Phillips*, 1956) and has now been achieved by GCMs for the very un-Earthlike environments of Titan and Venus (for examples see *Friedson et al.* 2009 and *Lebonnois et al.* 2010 respectively, and references therein). The case of Mars exemplifies a more practical goal. A credible model bridging the gap between local meteorology and global climatology aids both the choice of

spacecraft landing sites on Mars, and the interpretation of on-the-ground findings (e.g. *Haberle et al.*, 1999). Considering Earth, the most important challenge that GCMs face is predicting future climate over the next few decades and beyond. Put more precisely, the challenge is to gauge the strengths and weaknesses of GCMs, providing scientific background to the economic and political decisions that will be made about global warming. The models have already made and will continue to make predictions. Should we take these predictions seriously? Many considerations enter attempts to answer this question.

A necessary condition for believing predictions of future climate is a model's ability to simulate the present-day climate. Modern Earth GCMs produce temperature output including a seasonal cycle and large scale geographical variations that match observations to the level of 95% correlation; precipitation is more problematic, typically a 50 – 60% correlation with the observations, but simulations are improving and their overall global patterns are recognizably similar to observed patterns (see *Bader et al.*, 2008, especially their Figure 5.1). This provides some confidence in the largest scale GCM predictions of future precipitation trends (Figure SPM.7 in *IPCC*, 2007). In addition, GCMs produce a multi-year El Nino / Southern Oscillation (ENSO) with increasing accuracy (*AchutaRao and Sperber*, 2006). ENSO arises from natural ocean-atmosphere interactions in the tropics. Its spontaneous appearance in climate model output is important because ENSO is the leading mode of Earth's internally generated climate variability. Alongside naturally forced variations like those caused by volcanic eruptions (q.v.), internally generated variations like ENSO form the background "noise" against which human impacts on global climate must be assessed.

A more directly pertinent criterion for judging Earth GCMs is their ability to simulate global climate *changes* during the past. These include both natural phenomena such as the ice ages (*Rohling et al.*, 2012; *Hansen et al.*, this volume) and more recent changes, in particular the global warming observed over recent decades and thought “very likely due to the observed increase in anthropogenic greenhouse gas concentrations” (*IPCC*, 2007). Figure 7 shows both observations and GCM simulations of zonally averaged temperature trends since 1979. The observations include three different groups’ processing of microwave emissions recorded by a series of satellites. Different observing groups obtain somewhat divergent results from the same satellite data due to different assumptions regarding instrument calibrations, orbit decay effects, etc. Three broad levels of the atmosphere are observed: the lower troposphere, mid- to upper-troposphere and lower stratosphere ($z \sim 0 - 8$ km, $0 - 18$ km and $14 - 29$ km respectively; see Table 2 in *Karl et al.*, 2006). The model output has been processed to give the temperatures that satellites would observe over exactly the same altitude ranges, thus enabling an “apples to apples” comparison with the observations.

Figure 7 shows all models and all observations exhibiting a warming trend ($dT/dt > 0$) in the lower troposphere and a cooling trend ($dT/dt < 0$) in the lower stratosphere over more than 30 years at virtually all latitudes. Stratospheric cooling along with near-surface warming is the expected signature of an enhanced greenhouse effect, since increased greenhouse gases in the upper atmosphere lead to increased cooling to space. The lower tropospheric trends in Figure 7 represent better consistency than earlier comparisons in which surface observations and GCM simulations indicated significant warming, while satellite observations of the lower troposphere indicated no significant

temperature change (*Christy and McNider, 1994*)—leading to suggestions that one of the two classes of observation was systematically erroneous. The qualitative consistency of lower tropospheric temperature trends implied by Figure 7 is confirmed by analyses of *in situ* surface observations (most recently by *Wickham et al., 2013*).

Despite this qualitative agreement between models and observations, Figure 7 shows that throughout the troposphere within $\sim 40^\circ$ latitude of the Equator, nearly all models simulate a faster rate of warming than indicated by the observations. Time series of globally averaged near-surface temperature also show this quantitative discrepancy: both models and observations exhibit fairly steady warming over the past 35 years, but the overall rate of warming is greater in the models (J. R. Christy, personal communication). Many different explanations for the discrepancy are possible. We believe the following possibilities warrant special attention:

1. The models generally overestimate positive feedbacks and / or underestimate negative feedbacks, thereby overestimating Earth's equilibrium climate sensitivity $\Delta T_{2\times\text{CO}_2}$. This would be a serious indictment of the models and would make global warming a less worrisome problem than conventionally thought.
2. Climate models estimate $\Delta T_{2\times\text{CO}_2}$ correctly but overestimate the rate of warming as Earth adjusts to a new equilibrium state. This would also be a serious indictment of the models, possibly connected with an underestimate of natural internal oscillations of the climate system, e.g. those arising in the ocean with its enormous heat capacity. This model

deficiency could make global warming less worrisome, although warming of the magnitude that models predict could still be “in the pipeline.”

3. Forcing factors are missing or inaccurately represented in the models, causing the net climate forcing ΔF to be overestimated. Some models do not include volcanic effects on climate, which leads to a noticeable overestimate of ocean warming (see Figure 1c in *Gleckler et al.*, 2012). Inaccurate accounting of O₃ depletion in the lower stratosphere may also affect model-simulated temperature trends (*Santer et al.*, 2013). This type of error would be a much less serious indictment of the models because it could be corrected by more accurate input. It might or might not make global warming less worrisome. For example, if model input needs to be corrected by increasing the magnitude of negative forcing due to sulfate pollution (Section 2.3.1) then simulated current rates of warming would become less, but future rates of warming would become greater if the pollution is reduced.
4. The observational errors are underestimated. Figure 7—representing the most recent work at the time of writing this chapter—includes error estimates for only one of the three versions of the observations (5 – 95 percentiles for RSS). This suggests that identification and quantification of observational uncertainties is still in early days. Future work may well expand the observational “error bars.” This would lessen the degree of discrepancy between models and observations.

4. CONCLUSION

The subject of the greenhouse effect and climate feedbacks, put in the context of comparative climatology of terrestrial planets, is broad enough for several books like this volume. In this chapter we have focused on basic principles. Observations of Earth and other worlds in the Solar System leave no doubt that the greenhouse effect can significantly increase surface temperature. The theory of human-induced global warming on Earth follows naturally from the observations.

The same theory, however, concludes that poorly known processes such as those involving clouds translate into a wide margin of uncertainty about Earth's future climate. Although the power of computers and with it the complexity of climate models has increased enormously over the past few decades, uncertainty in the fundamental sensitivity parameter $\Delta T_{2\times\text{CO}_2}$ has not decreased—despite gratifying improvements in simulating the present-day climate, short term climate variations, recent (~ 100 yr) global warming, and paleoclimates. Current best estimates for the possible range of $\Delta T_{2\times\text{CO}_2}$ (see Box 10.2 in *Meehl et al.*, 2007) are not radically different from the 1.5 – 4.5 K range estimated by the first official report on human-induced global warming (*Charney*, 1979). The lower ends of this range might be tolerable for humanity; the higher estimate would put Earth into a state not seen for millions of years.

Reducing these uncertainties may require a different approach than incremental refinement of detailed Earth-centric models. To some extent this process is already underway. Global warming simulations are increasingly informed by paleoclimate simulations, which test the ability of models to explain a “different Earth” (*Jansen et al.*,

2007; *Hansen et al.*, this volume). Many extraterrestrial weather and climate models have evolved from Earth GCMs (Section 3.4). The extraterrestrial simulations certainly benefit from decades of Earth climate modeling. Now may be the time to expand the connections by building a “coherent” climate model that *simultaneously* represents several worlds at once (*Schmidt*, 2012).

Acknowledgments. We thank Amy Henke for graphic arts, John Christy for discussion of model evaluation, Phil Christensen for supplying the data for Figure 3, and Ben Santer for both discussions and preparing a special gray-scale version of Figure 7. This work was supported in part by NASA and conducted under auspices of the Office of Science, US Department of Energy, by Lawrence Livermore National Laboratory under Contract DE-AC52-07NA27344.

REFERENCES

- AchutaRao K. M. and K. R. Sperber (2006) ENSO simulation in coupled ocean-atmosphere models: Are the current models better? *Climate Dynamics*, 27, 1-15.
- Bader D. C., Covey C., Gutowski W. J., Held I. M., Kunkel K. E., Miller R. L, Tokmakian R. T. and Zhang M. H. (2008) *Climate Models: An Assessment of Strengths and Limitations*. U.S. Department of Energy, Washington, DC. Available at <http://www.climate-science.gov/Library/sap/sap3-1/final-report/sap3-1-final-all.pdf>.
- Boynton W.V., et al. (2002) Distribution of hydrogen in the near surface of Mars: Evidence for subsurface ice deposits. *Science*, 297, 81-85.
- Box G. E. P. and Draper N. R. (1987) *Empirical Model-Building and Response Surfaces*. Wiley, New York, 688 pp.
- Bullock M. A. and Grinspoon D. H. (2001) The recent evolution of climate on Venus. *Icarus*, 150, 19-37.
- Charney J. G. (1979) *Carbon Dioxide and Climate: A Scientific Assessment*. National Academy of Sciences, Washington, DC, 22 pp.
- Christensen, P. R., Anderson D. L., Chase S. C., Clancy R. T., Clark R. N., Kieffer H. H., Kuzmin R. O., Malin M. C., Pearl J. C., Roush T. L. and Smith M. D. (1998) Results from the Mars Global Surveyor thermal emission spectrometer. *Science*, 279, 1692-1698.

- Christy J. R. and McNider R. T. (1994) Satellite greenhouse signal. *Nature*, 367, 325-325.
- Courtin R., McKay C. P. and Pollack J. (1992) L'effet de serre dans le systeme solaire. *La Recherche*, 23, 542-549.
- Covey, C. and S. Klein (2010) *Plausible Ranges of Observed TOA Fluxes*, Lawrence Livermore National Laboratory Technical Report LLNL-TR-435351. Available at <https://e-reports-ext.llnl.gov/pdf/402766.pdf>.
- Crisp D. and Titov D. (1997) The thermal balance of the Venus atmosphere. In *Venus II: Geology, Geophysics, Atmosphere, and Solar Wind Environment* (S. W. Bougher, D. M. Hunten and R. J. Phillips, eds.), pp. 353-384. University of Arizona Press, Tuscon.
- Denman K. L., Brasseur G., Chidthaisong A., et al. (2007) Couplings Between Changes in the Climate System and Biogeochemistry. In: *Climate Change 2007: The Physical Science Basis. Contribution of Working Group I to the Fourth Assessment Report of the Intergovernmental Panel on Climate Change* [Solomon S. Qin D., Manning D., Chen Z., Marquis M., Averyt K. B., Tignor M. and Miller H. L. (eds.)]. Cambridge University Press, Cambridge, United Kingdom and New York, NY, USA.
- Dickinson R. E. and Cicerone R. J. (1986) Future global warming from atmospheric trace gases. *Nature*, 319, 109-115.
- Eyring V., Shepherd T. G. and Waugh D. W., eds. (2010) *Chemistry-climate Model Validation*. SPARC Rep. 5, WCRP-30, WMO/TD-40, 194 pp. Available at www.sparc-climate.org/publications/sparc-reports/sparc-report-no5..

- Forster P., Ramaswamy V., Artaxo P., et al. (2007) Changes in Atmospheric Constituents and in Radiative Forcing. In: *Climate Change 2007: The Physical Science Basis. Contribution of Working Group I to the Fourth Assessment Report of the Intergovernmental Panel on Climate Change* [Solomon S., D. Qin, M. Manning, Z. Chen, M. Marquis, K.B. Averyt, M. Tignor and H.L. Miller (eds.)]. Cambridge University Press, Cambridge, United Kingdom and New York, NY, USA.
- Fasullo J. T. and Trenberth K. E. (2008) The annual cycle of the energy budget. Part II: Meridional structures and poleward transports. *J. Climate*, 21, 2313-2325.
- Fourier J. (1827) Memoire sur la temperature du globe terrestre et des espaces planetaires. *Memoirs of the Royal Academy of Sciences of the Institut de France*, pp. 569-604. English translation at http://www.wmconnolley.org.uk/sci/fourier_1827/fourier_1827.html.
- Friedson A. J., West R. A., Wilson E. H., Oyafuso F. and Orton G. S. (2009) A global climate model of Titan's atmosphere and surface. *Planetary and Space Science*, 57, 1931-1949.
- Fulchignoni M., Ferri F., Angrilli F., et al. (2005) In situ measurements of the physical characteristics of Titan's environment. *Nature*, 438, 785-791.
- Gerber E. P., Butler A., Calvo N., et al. (2012) Assessing and understanding the impact of stratospheric dynamics and variability on the Earth system. *Bull. Amer. Meterol. Soc.*, 93, 845-859.
- Gierasch P. J., Goody R. M., Young R. E., Crisp D., Edwards C., Kahn R., McCleese D., Rider D., Del Genio A., Greely R., Hou A., Leovy C. B. and Newman M. (1997)

- The general circulation of the Venus atmosphere: An assessment. In *Venus II: Geology, Geophysics, Atmosphere, and Solar Wind Environment* (S. W. Bougher, D. M. Hunten and R. J. Phillips, eds.), pp. 459-500. Univ. Arizona Press, Tuscon, AZ.
- Gleckler P. J., Wigley T. M. L., Santer B. D., Gregory J. M., AchutaRao K. and Taylor K. E. (2006) Volcanoes and climate: Krakatoa's signature persists in the ocean. *Nature*, 439, 675.
- Gleckler P. J., Santer B. D., Domingues C. M., Pierce D. W., Barnett T. P., Church J. A., Taylor K. E., AchutaRao K. M., Boyer T. P., Ishii M. and Caldwell P. M. (2012) Human-induced global ocean warming on multidecadal timescales. *Nature Climate Change*, 2, 524-529.
- Goudie A. S. and Viles, H. A. (2012) Weathering and the global carbon cycle: Geomorphological perspectives. *Earth-Science Reviews*, 113, 59-71.
- Griffith C. A. (2009) Storms, polar deposits and the methane cycle in Titan's atmosphere. *Phil. Trans. Roy. Soc. A* 367, 713-728.
- Haberle, R. M., Joshi, M. M., Murphy, J. R., Barnes, J. R., Schofield, J. T., Wilson G. R., Lopez-Valverde M., Hollingsworth J. L., Bridger A. F. C. and Schaeffer J. (1999). GCM Simulations of the Mars Pathfinder ASI/MET Data. *J. Geophys. Res.*, 104, 8957-8974.
- Haberle R. M., and the NASA/Ames Mars General Circulation Modeling Group (2010) Modeling the seasonal water cycle on Mars: Implications for sources and sinks. AGU Fall Meeting abstract P51E-01. Available at http://www.agu.org/meetings/fm10/fm10-sessions/fm10_P51E.html.

- Haberle R. M., Kahre M. A., Hollingsworth J. L., Schaeffer J., Montmessin F. and Phillips R. J. (2012). A cloud greenhouse effect on Mars: Significant climate change in the recent past? 43rd Lunar and Planet. Sci. Conf., LPI Contribution No. 1659, id.1665.
- Haberle R. M., Forget F., Head J., Kahre M. A. and Kreslavsky M. (2013) Summary of the Mars recent climate change workshop, NASA Ames Research Center, May 15 – 17, 2012. *Icarus* 222, 415-418.
- Haberle R. M. (2013) Estimating the power of Mars' greenhouse effect. *Icarus*, in press.
- Hanel R. A., Schlachman B., Rogers D. and Vanous D. (1971) Nimbus 4 Michelson interferometer, *Appl. Optics*, 10, 1376-1882.
- Hanel, R., Conrath B., Flasar F. M., Kunde V., Maguire W., Pearl J., Pirraglia J., Samuelson R., Herath L., Allison M., Cruikshank D., Gautier D., Gierasch P., Horn L., Koppany R. and Ponnampereuma C. (1981) Infrared observations of the Saturnian system from Voyager 1. *Science* 212, 192-200.
- Hanel, R., Conrath B., Flasar F. M., Kunde V., Maguire W., Pearl J., Pirraglia J., Samuelson R., Cruikshank D., Gautier D., Gierasch P., Horn L. and Ponnampereuma C. (1982) Infrared observations of the Saturnian system from Voyager 2. *Science* 215, 544-548.
- Hansen J., Johnson D., Lacis A., Lebedeff S., Lee P., Rind D. and Russell G. (1981) Climate impact of increasing atmospheric carbon dioxide. *Science*, 213, 957-966.

- Hartmann W. K. (2005) *Moons and Planets*, 5th ed. Books / Cole, Belmont, CA, 428 pp.
- Houghton J. (2002) *The Physics of Atmospheres*, 3rd ed. Cambridge Univ. Press, Cambridge, 340 pp.
- Hunten, D. M. and Goody R. M. (1969) Venus: The next phase of planetary exploration. *Science* 165, 1317-1323.
- Ingersoll A. P. (1969) The runaway greenhouse: A history of water vapor on Venus. *J. Atmos. Sci.*, 26, 1191-1198.
- IPCC (2007) Summary for Policymakers. In: *Climate Change 2007: The Physical Science Basis. Contribution of Working Group I to the Fourth Assessment Report of the Intergovernmental Panel on Climate Change* [Solomon S. Qin D., Manning D., Chen Z., Marquis M., Averyt K. B., Tignor M. and Miller H. L. (eds.)]. Cambridge University Press, Cambridge, United Kingdom and New York, NY, USA.
- Jansen, E., Overpeck J., Briffa K. R., et al. (2007) Palaeoclimate. In: *Climate Change 2007: The Physical Science Basis. Contribution of Working Group I to the Fourth Assessment Report of the Intergovernmental Panel on Climate Change* [Solomon S. Qin D., Manning D., Chen Z., Marquis M., Averyt K. B., Tignor M. and Miller H. L. (eds.)]. Cambridge University Press, Cambridge, United Kingdom and New York, NY, USA.
- Jones P. D., New M., Parker D. E., Martin S. and Rigor I. G. (1999) Surface air temperature and its variations over the last 150 years. *Reviews of Geophysics* 37, 173-199.

- Karl T. R., Hassol S. J., Miller C. D. and Murray W. L., eds. (2006) *Temperature Trends in the Lower Atmosphere: Steps for Understanding and Reconciling Differences*. National Oceanic and Atmospheric Administration, Washington, DC.
- Available at <http://www.climate-science.gov/Library/sap/sap1-1/finalreport/sap1-1-final-frontmatter.pdf>.
- Kieffer H. and Zent A.P. (1992) Quasi-periodic climate change on Mars. In Mars (H. H. Kieffer et al., eds. *Mars*, pp. 180-1233. Univ. Arizona Press, Tuscon, AZ.
- Kim M. and Ramanathan V. (2012) Improved estimates and understanding of global albedo and atmospheric solar absorption. *Geophys. Res. Lett.*, 39, L24704.
- Komabayashi M. (1967) Discrete equilibrium temperatures of a hypothetical planet with the atmosphere and the hydrosphere of one component-two phase system under constant solar radiation. *J. Meteor. Soc. Japan* 45, 137-139.
- Kurokawa H. and Nakamoto T. (2012) Effects of atmospheric absorption of incoming radiation on the radiation limit of the troposphere. *J. Atmos. Sci.*, 69, 403-413.
- Laskar J. Correia A.C.M., Gastineau M., Joutel F. Levrard B. and Robutel, P. (2004) Long term evolution and chaotic diffusion of the insolation quantities of Mars. *Icarus*, 170, 343-364.
- Lebonnois S., Hourdin F., Eymet V., Cresspin A., Fournier R. and Forget F. (2010) Superrotation of Venus' atmosphere analyzed with a full general circulation model. *J. Geophys. Res. (Planets)*, 115, E06006, 23 pp.
- Leighton R. B. and Murray B.C. (1966) Behavior of carbon dioxide and other volatiles on Mars. *Science*, 153, 136-144.

- Lindzen R. S. and Emanuel K. (2002) The greenhouse effect. In the *Encyclopedia of Global Change* (J. R. Holton, ed.), pp. 562-566. Oxford University Press, New York.
- Loeb N. G., Wielicki B. A., Doelling D. R., Smith G. L., Keyes D. F., Kato S., Manalo-Smith N. and Wong T. (2009) Toward optimal closure of the Earth's top-of-atmosphere radiation budget. *J. Climate*, 22, 748-766.
- Madeleine J.-B., Head J. W., Forget F., Navarro T., Millour E., Spiga A., Colaitis A., Montmesson F., Määttänen A. (2013). What defines a Martian glacial sate? Analysis of the Mars climate system under past conditions using the new LMD Global Climate Model. 44th Lunar and Planet. Sci. Conf. LPI Contribution No. 1719, p. 1895.
- Manabe S. and Weatherald R. T. (1967) Thermal equilibrium of the atmosphere with a given distribution of relative humidity. *J. Atmos. Sci.*, 24, 241-259.
- McKay C. P., Pollack J. B. and Courtin R. (1992) The greenhouse and antigreenhouse effects on Titan. *Science*, 253, 1118-1121.
- McComiskey, A. and Feingold, G., 2012. The scale problem in quantifying aerosol indirect effects. *Atmospheric Chemistry and Physics*, 12, 1031-1049.
- Marinova M. M., McKay C. P. and Hashimoto H. (2005) Radiative-convective model of warming Mars with artificial greenhouse gases. *J. Geophys. Res. (Planets)* 110, E03002, doi:10.1029/2004JE002306.
- Meehl G.A., Stocker T. F., Collins W. D., et al. (2007) Global Climate Projections. In: *Climate Change 2007: The Physical Science Basis. Contribution of Working Group I to the Fourth Assessment Report of the Intergovernmental Panel on*

- Climate Change* [Solomon S., D. Qin, M. Manning, Z. Chen, M. Marquis, K.B. Averyt, M. Tignor and H.L. Miller (eds.)]. Cambridge University Press, Cambridge, United Kingdom and New York, NY, USA.
- Mitchell J. L. (2012) Titan's transport-driven methane cycle. *Ap. J. Lett.*, 756, L26 (5 pp).
- Penner J. E., Xu L. and Wang M. H. (2011) Satellite methods underestimate indirect climate forcing by aerosols. *Proc. National Acad. Sci. USA*, 108, 13404-13408.
- Phillips N. A. (1956) The general circulation of the atmosphere: A numerical experiment. *Quarterly Journal of the Royal Meteorological Society*, 82, 123-164.
- Phillips, R., et al. (2011) Massive CO₂ ice deposits sequestered in the south polar layered deposits of Mars. *Science*, 332, 838-841.
- Pollack J. B., Toon O. B. and Boese R. (1980) Greenhouse models of Venus' high surface temperature, as constrained by Pioneer Venus measurements. *J. Geophys. Res.*, 85, 8223-8231.
- Pollack J. B., Toon O. B., Ackerman T. P., and McKay C. P. (1983) Environmental effects of an impact-generated dust cloud: Implications for the Cretaceous-Tertiary Extinctions. *Science*, 219, 287-289.
- Pollack J. B., Kasting J. F., Richardson S. M. and Poliakoff (1987) The case for a wet, warm climate on early Mars. *Icarus*, 71, 203-224.
- Pierrehumbert R. T. (2011) Infrared radiation and planetary temperature. *Physics Today*, 64, 33-38.

- Ramanathan V. and Coakley J. A. (1978) Climate modeling through radiative-convective models. *Rev. Geophys. Space Phys.*, 16, 465-489.
- Read P. L. and Lewis S. R. (2004) *The Martian Climate Revisited: Atmosphere and Environment of a Desert Planet*. Springer, Berlin. 352 pp.
- Revelle, R., and H. Suess (1957) Carbon dioxide exchange between atmosphere and ocean and the question of an increase of atmospheric CO₂ during the past decades. *Tellus* 9, 18-27.
- Robock A. (2011) Nuclear winter is a real and present danger. *Nature*, 473, 275-276.
- Rohling E. J., Sluijs A., Dijkstra H. A., et al. (2012) Making sense of paleoclimate sensitivity. *Nature*, 491, 683-691.
- Samuelson R. E., Hanel R. A., Kunde V. G. and Maguire W. C. (1981) Mean molecular weight and hydrogen abundance of Titan's atmosphere. *Nature*, 292, 688-693.
- Samuelson R. E., Maguire W. C., Hanel R. A., Kunde V. G., Jennings D. E., Yung Y. L. and Aikin A. C. (1983) CO₂ on Titan. *J. Geophys. Res.*, 88, 8709-8715.
- Santer B. D., Painter J. F., Mears C. A., et al. (2013) Identifying human influences on atmospheric temperature. *Proc. National Acad. Sci. USA*, 110, 26-33.
- Schmidt G. A., Ruedy R. A., Miller R. M. and Lacis A. A. (2010) Attribution of the present-day total greenhouse effect. *Geophys. Res. Lett.*, 115, D20106.
- Schmidt G. A. (2012) Issues in building a coherent climate model for terrestrial planets. Abstract for the Comparative Climatology of Terrestrial Planets workshop, Boulder, CO, 25-28 June. Available at <http://www.lpi.usra.edu/meetings/climatology2012/pdf/8088.pdf>.

- Schofield J. T. and Taylor F. W. (1982) Net global thermal emission for the venusian upper atmosphere. *Icarus*, 52, 245-262.
- Schubert G. (1983) General circulation and the dynamical state of the Venus atmosphere. In *Venus* (D. M. Hunten, L. Colin, T. M. Donahue and V. I. Moroz, eds.), pp. 681-765. Univ. Arizona Press, Tuscon, AZ.
- Shaviv N. J., Shaviv G. and Wehrse R. (2011) The maximal runaway temperature of earth-like planets. *Icarus*, 216, 403-415.
- Solomon S., Qin D., Manning M., et al. (2007) Technical summary. In: *Climate Change 2007: The Physical Science Basis. Contribution of Working Group I to the Fourth Assessment Report of the Intergovernmental Panel on Climate Change* [Solomon S., D. Qin, M. Manning, Z. Chen, M. Marquis, K.B. Averyt, M. Tignor and H.L. Miller (eds.)]. Cambridge University Press, Cambridge, United Kingdom and New York, NY, USA.
- Stevens B. and Boucher O. (2012) The aerosol effect. *Nature*, 490, 40-41.
- Titov D. V., Bullock M. A., Crisp D., Renno N. O., Taylor F. W., and Zasova L. V. (2007) Radiation in the atmosphere of Venus. In *Exploring Venus as a Terrestrial Planet*. Geophysical Monograph Series, vol. 176, 225 pp. [L. W. Esposito, E. R. Stofan, and T. E. Cravens (Eds.)] 121-138.
- Titov D. V., Drossart P., Piccioni G. and Markiewicz W. J. (2013) Radiative energy balance in the Venus atmosphere. In *Towards Understanding the Climate of Venus: Applications of Terrestrial Models to Our Sister Planet*. ISSI Scientific Report Series, Vol. 11 [Bengtsson, L.; Bonnet, R.-M.; Grinspoon, D.; Koumoutsaris, S.; Lebonnois, S.; Titov, D. (Eds.)] pp. 23-49. Springer.

- Toon O. B., Pollack J. B., Ward W., Burns J. A. and Bilski K. (1980) The astronomical theory of climate change on Mars. *Icarus*, 44, 552-607.
- Toon O. B., Zahnle K., Morrison D., Turco R. and Covey C. (1997) Environmental perturbations caused by the impacts of asteroids and comets. *Rev. Geophys.*, 35, 41-78.
- Trenberth K. E. and Fasullo J. T. (2010) Tracking Earth's energy. *Science*, 328, 316-317.
- Turco R., Toon O. B., Ackerman T. P., Pollack J. B. and Sagan C. (1983) Nuclear winter: Global consequences of multiple nuclear explosions. *Science*, 222, 1283-1292.
- Tyndall, J. (1873). *Contributions to Molecular Physics in the Domain of Radiant Heat*. Forgotten Books, 462 pp. Also available at <http://archive.org/details/contributionsto02tyndgoog>.
- Walker J. C. G., Hays P. B. and Kasting J. F. (1981) A negative feedback mechanism for the long-term stabilization of Earth's surface temperature. *J. Geophys. Res.*, 86, 9776-9782.
- Washington W. M. and C. L. (2005) *An Introduction to Three-Dimensional Climate Modeling, 2nd ed.* University Science Books, Sausalito, CA. 353 pp.
- Wickham C., Rohde R., Muller R., et al. (2013) Influence of urban heating on the global temperature land average using rural sites identified from MODIS classifications. *Geoinformation and Geostatistics*, 1, 1-6 (<http://dx.doi.org/10.4172/gigs.1000104>).

Wood S. F., Griffiths S. D., Bapst J. N. (2012) Mars at low obliquity: Perennial CO₂ caps, atmospheric collapse, and subsurface warming. NASA/CP-20120216054, p. 44-47. Available at <http://spacescience.arc.nasa.gov/mars-climate-workshop-2012>.

TABLE 1. Earthlike worlds with substantial atmospheres.

<i>Planet / Moon</i>	Solar flux (S)	Planetary Albedo (α)	Effective T (T_e)	Surface T (T_{sfc})
Venus	2599 W m ⁻²	0.76	230 K	730 K
Earth	1361 W m ⁻²	0.30	255 K	288 K
Mars*	586 W m ⁻²	0.24	210 K	204 K
Titan	15 W m ⁻²	0.3	82 K	94 K

*Mars α and T_{sfc} values are from the NASA ARC Mars GCM; $T_{sfc} < T_e$ due to strong diurnal cycle and nonlinear Planck function (*Haberle, 2013*).

TABLE 2. Human radiative forcing of Earth's climate (*Forster et al., 2007*).*

<i>Forcing Agent</i>	Best Estimate	90% Confidence Interval
CO ₂	1.66 W m ⁻²	1.49 to 1.83 W m ⁻²
CH ₄	0.48 W m ⁻²	0.43 to 0.53 W m ⁻²
N ₂ O	0.16 W m ⁻²	0.14 to 0.18 W m ⁻²
Chlorofluorocarbons	0.34 W m ⁻²	0.31 to 0.37 W m ⁻²
Tropospheric O ₃	0.35 W m ⁻²	0.25 to 0.65 W m ⁻²
Stratospheric O ₃	-0.04 W m ⁻²	-0.15 to +0.05 W m ⁻²
Land use change	-0.20 W m ⁻²	-0.40 to 0.00 W m ⁻²
Direct H ₂ SO ₄ aerosol	-0.40 W m ⁻²	-0.60 to -0.20 W m ⁻²
Aerosol / cloud albedo	-0.70 W m ⁻²	-1.10 to +0.40 W m ⁻²

*Considering increases from the beginning of the Industrial Revolution (c. 1750) to 2005.

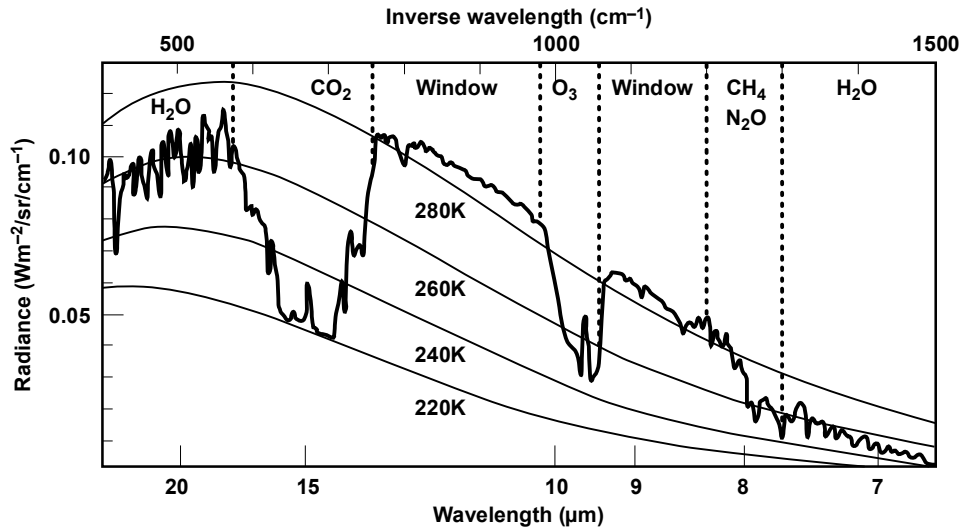


Figure 1. Intensity of outgoing IR as a function of wavelength, as observed by the Nimbus 4 satellite over the Mediterranean Sea. Clouds were not present in this area at the time of observation. Smooth lines give Planck blackbody IR emission intensities at selected temperatures. Principal molecular IR-absorption bands are indicated. In the “window” regions outside these bands, outgoing IR intensity comes directly from the sea surface with temperature slightly greater than 280 K. Redrawn from *Houghton* (2009).

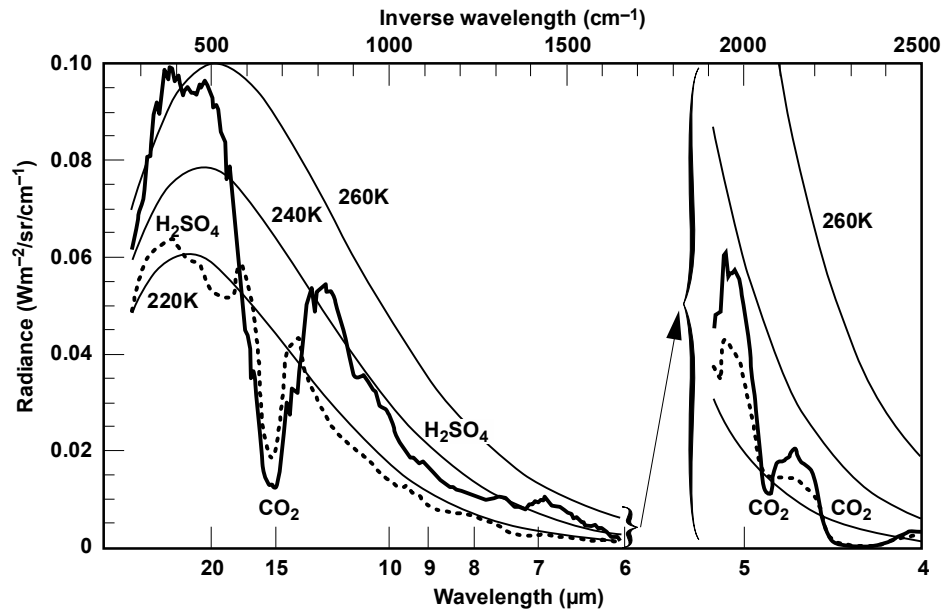


Figure 2. Same as Figure 1 for Venus, observed by the Venera 15 and Galileo spacecraft over the equator (solid lines) and higher latitudes (dotted lines). Outgoing intensities from near-IR wavelengths (right side) are multiplied by a factor 100. Redrawn from *Titov et al. (2007)*.

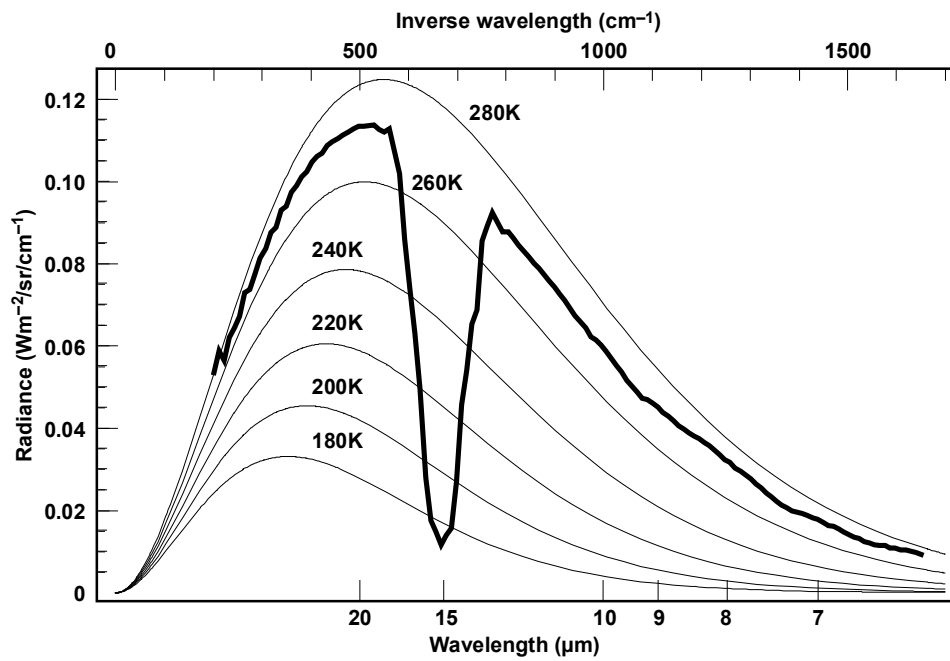
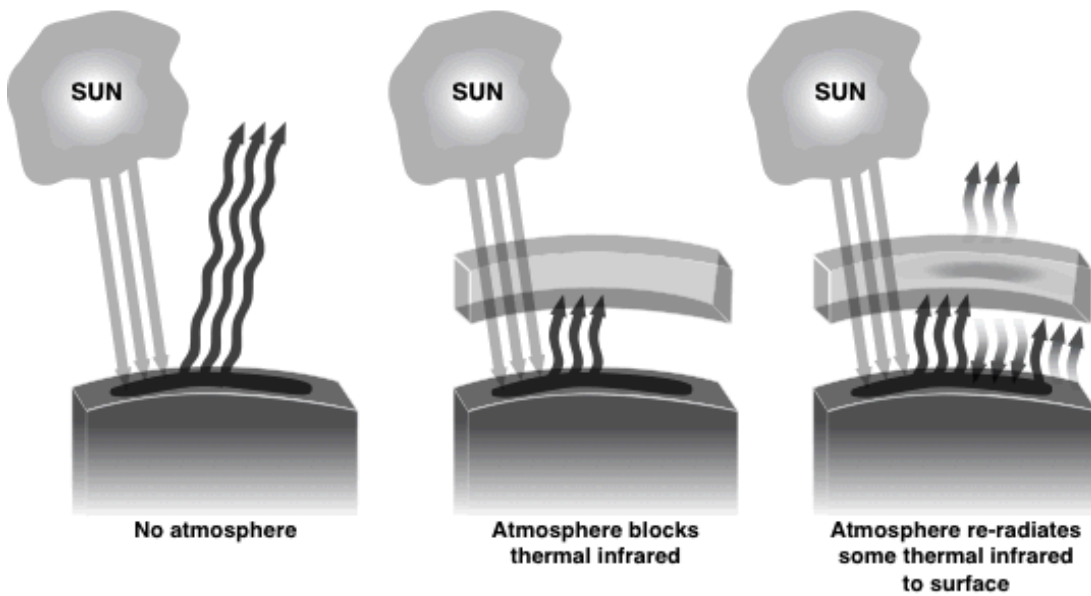


Figure 3. Same as Figures 1 – 2 for Mars, observed by the Mars Global Surveyor spacecraft over a cloud-free area in summer (*Christensen et al., 1998*).

THE GREENHOUSE EFFECT



THE ANTI-GREENHOUSE EFFECT

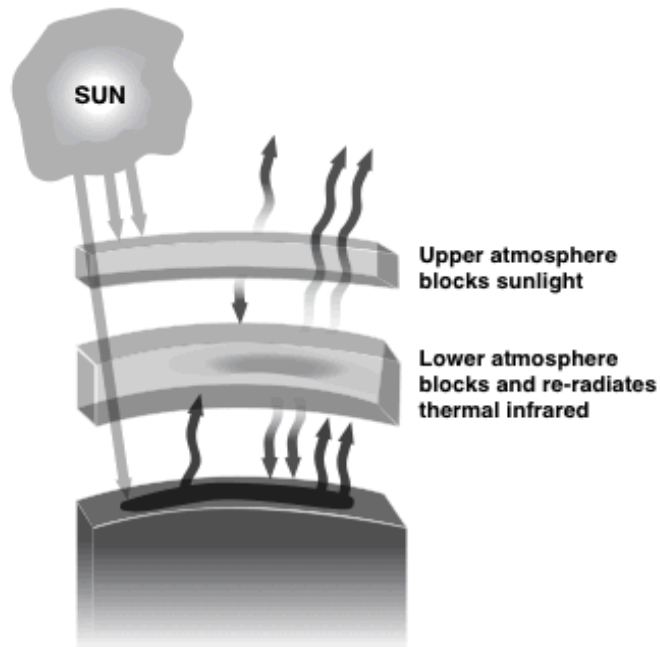
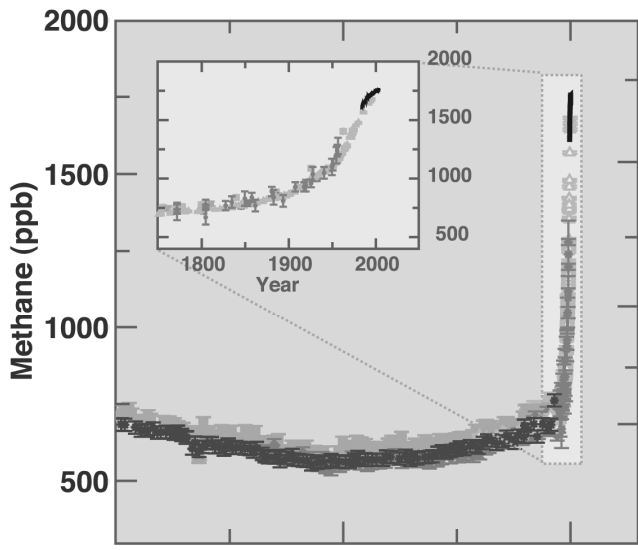
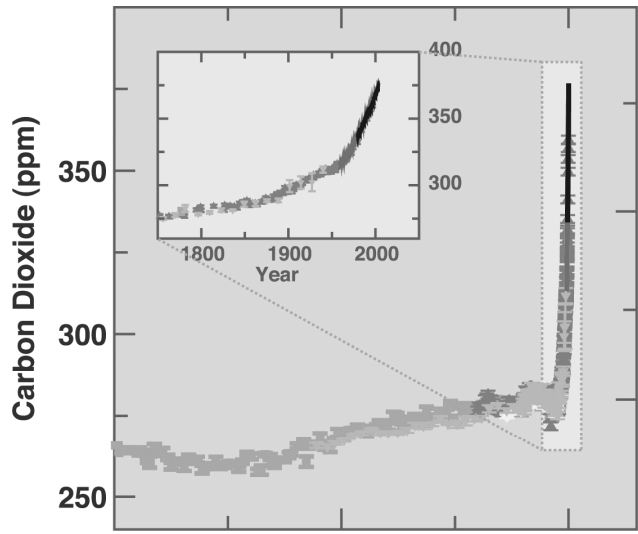


Figure 4. Schematic comparison of the greenhouse effect (top pictures) with the anti-greenhouse effect (bottom picture). Gray arrows denote solar radiation, black arrows denote infrared radiation, and the number of arrows indicate the relative sizes of energy fluxes.



©IPCC 2007: WG1-AR4

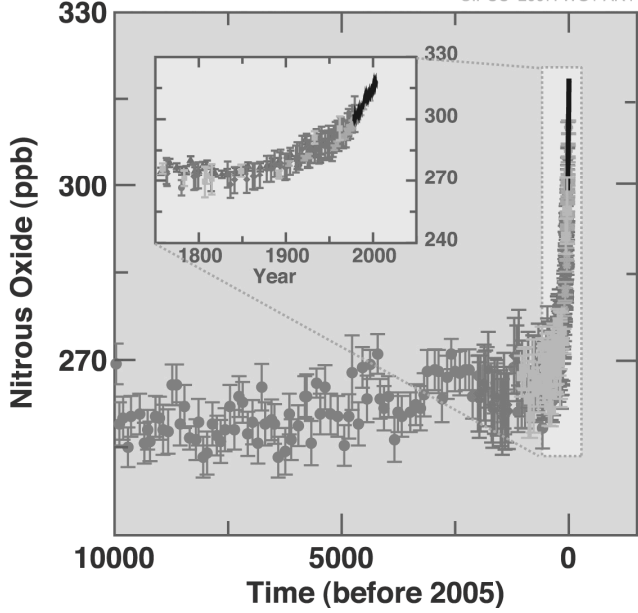


Figure 5. Atmospheric concentrations of the primary well-mixed greenhouse gases in Earth's atmosphere over the last 10,000 years (large panels) and since 1750 (inset panels). Points with error bars are measurements from ice cores, with different gray shading indicating different studies. Black lines beginning c.1950 are direct atmospheric measurements. Redrawn from *Jansen et al. (2007) Figure 6.4*; the original color figure extends over the last 20,000 years, identifies the different studies, and also shows the corresponding radiative forcing (see text).

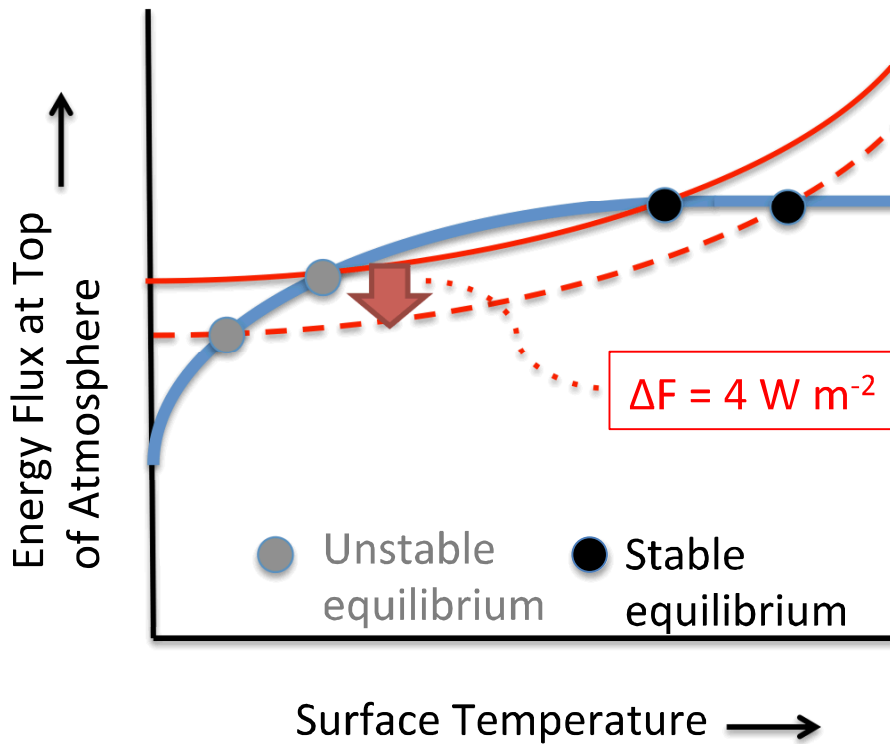


Figure 6. Schematic of outgoing IR energy fluxes (upward-curving lines) and absorbed solar energy fluxes (downward curving line) as a function of global mean surface temperature. Outgoing IR curves upward with increasing temperature unless a runaway greenhouse exists. Absorbed solar energy increases with temperature but asymptotes at high temperatures if snow- and ice-albedo feedback dominates. A hypothetical sudden doubling of atmospheric carbon dioxide lowers outgoing IR by $\sim 4 \text{ W m}^{-2}$, as shown in the change from solid to dashed line for outgoing IR.

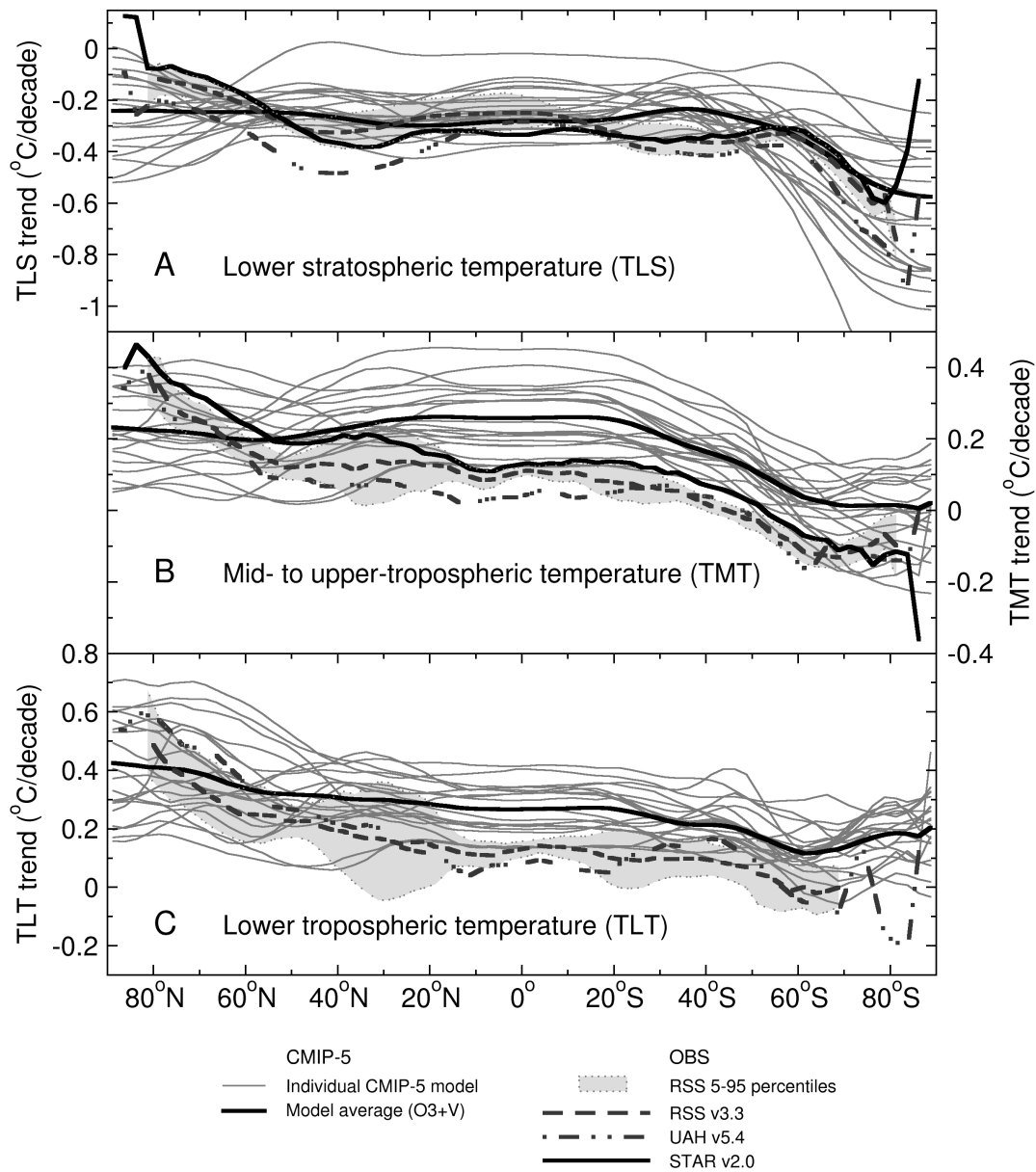


Figure 7. Zonal mean satellite-observed temperature trends, 1979 – 2011, shown as a function of latitude for three atmospheric levels together with corresponding model-simulated trends. Redrawn from *Santer et al. (2013)* Figure 3; the original color figure identifies the different model simulations.